

**Manuscript version: Published Version**

The version presented in WRAP is the published version (Version of Record).

**Persistent WRAP URL:**

<http://wrap.warwick.ac.uk/175245>

**How to cite:**

The repository item page linked to above, will contain details on accessing citation guidance from the publisher.

**Copyright and reuse:**

The Warwick Research Archive Portal (WRAP) makes this work by researchers of the University of Warwick available open access under the following conditions.

Copyright © and all moral rights to the version of the paper presented here belong to the individual author(s) and/or other copyright owners. To the extent reasonable and practicable the material made available in WRAP has been checked for eligibility before being made available.

Copies of full items can be used for personal research or study, educational, or not-for-profit purposes without prior permission or charge. Provided that the authors, title and full bibliographic details are credited, a hyperlink and/or URL is given for the original metadata page and the content is not changed in any way.

**Publisher's statement:**

Please refer to the repository item page, publisher's statement section, for further information.

For more information, please contact the WRAP Team at: [wrap@warwick.ac.uk](mailto:wrap@warwick.ac.uk)

# Ice nucleation in aqueous solutions of short- and long-chain poly(vinyl alcohol) studied with a droplet microfluidics setup

Cite as: J. Chem. Phys. 158, 154504 (2023); doi: 10.1063/5.0136192

Submitted: 24 November 2022 • Accepted: 22 February 2023 •

Published Online: 17 April 2023











View Online



Export Citation



CrossMark

Lukas Eickhoff,<sup>1</sup>  Mira Keßler,<sup>1</sup>  Christopher Stubbs,<sup>2</sup>  Jakob Derksen,<sup>3,a)</sup> Martina Viefhues,<sup>3</sup>   
Dario Anselmetti,<sup>3</sup>  Matthew I. Gibson,<sup>2,4</sup>  Berthold Hoge,<sup>1</sup>  and Thomas Koop<sup>1,b)</sup> 

## AFFILIATIONS

<sup>1</sup> Faculty of Chemistry, Bielefeld University, 33615 Bielefeld, Germany

<sup>2</sup> Department of Chemistry, University of Warwick, Coventry CV4 7AL, United Kingdom

<sup>3</sup> Faculty of Physics, Bielefeld University, 33615 Bielefeld, Germany

<sup>4</sup> Division of Biomedical Sciences, Warwick Medical School, University of Warwick, Coventry CV4 7AL, United Kingdom

**Note:** This paper is part of the JCP Special Topic on Nucleation: Current Understanding Approaching 150 Years After Gibbs.

<sup>a)</sup> **Now at:** School of Life Sciences, University of Siegen, 57076 Siegen, Germany.

<sup>b)</sup> **Author to whom correspondence should be addressed:** [thomas.koop@uni-bielefeld.de](mailto:thomas.koop@uni-bielefeld.de)

## ABSTRACT

Poly(vinyl alcohol) (PVA) has ice binding and ice nucleating properties. Here, we explore the dependence of the molecular size of PVA on its ice nucleation activity. For this purpose, we studied ice nucleation in aqueous solutions of PVA samples with molar masses ranging from 370 to 145 000 g mol<sup>-1</sup>, with a particular focus on oligomer samples with low molar mass. The experiments employed a novel microfluidic setup that is a follow-up on the previous Weizmann Supercooled Droplets Observation on a Microarray (WISDOM) design by Reicher *et al.* The modified setup introduced and characterized here, termed nanoliter Bielefeld Ice Nucleation ARraY (nanoBINaRY), uses droplet microfluidics with droplets (96 ± 4) μm in diameter and a fluorinated continuous oil phase and surfactant. A comparison of homogeneous and heterogeneous ice nucleation data obtained with nanoBINaRY to those obtained with WISDOM shows very good agreement, underpinning its ability to study low-temperature ice nucleators as well as homogeneous ice nucleation due to the low background of impurities. The experiments on aqueous PVA solutions revealed that the ice nucleation activity of shorter PVA chains strongly decreases with a decrease in molar mass. While the cumulative number of ice nucleating sites per mass  $n_m$  of polymers with different molar masses is the same, it becomes smaller for oligomers and completely vanishes for dimer and monomer representatives such as 1,3-butanediol, propan-2-ol, and ethanol, most likely because these molecules become too small to effectively stabilize the critical ice embryo. Overall, our results are consistent with PVA polymers and oligomers acting as heterogeneous ice nucleators.

Published under an exclusive license by AIP Publishing. <https://doi.org/10.1063/5.0136192>

## I. INTRODUCTION

Micrometer-sized liquid droplets of clean water without contaminants can be cooled without freezing to temperatures of about -38 °C before homogeneous ice nucleation, and subsequent crystallization of macroscopic ice crystals occurs.<sup>1-3</sup> However, when such droplets contain ice nucleating particles, the freezing process is catalyzed and, thus, freezing occurs at higher temperatures somewhere between -38 °C and the ice melting point.<sup>4</sup> This process, called heterogeneous ice nucleation, is relevant for many biological and atmospheric processes.<sup>5-7</sup> In the Earth's atmosphere, heterogeneous

ice nucleation is a ubiquitous process, in which the freezing temperature of atmospheric water droplets is influenced by many different types of insoluble ice nucleating particles, such as biological particles or mineral dust.<sup>8-12</sup>

Recent studies have shown that macromolecules dissolved in water or aggregates of smaller molecules can also act as ice nucleating molecules (INM) under certain conditions.<sup>10,13-20</sup> Relevant criteria for a high-temperature INM are, for example, the size of the ice nucleating molecule on the one hand and the strength of its interaction with the surface of a newly formed ice embryo on the other hand.<sup>10,13,15-18,21,22</sup> These studies suggest that the activity

of ice nucleating molecules increases with their size, which can be achieved either by increasing the length of the dissolved molecules or by aggregation of several molecules, for example, by solute–solvent interaction in a solution or by covalent bonding during synthesis.<sup>10,13,15–19,23</sup>

In nature, many of the known INMs are proteins, and these ice nucleating proteins are considered to form a subgroup of so-called ice binding proteins (IBPs), which are proteins that can bind to specific surfaces of ice crystals. Originally, this group of IBPs consisted of natural so-called antifreeze proteins (AFPs), which control the rate of ice crystal growth or inhibit ice recrystallization by adsorption to existing ice crystals.<sup>24,25</sup> AFPs are omnipresent in the flora and fauna of polar and other cold regions and they prevent cell damage of organisms by inhibiting the growth of small ice crystals within the cells of their host.<sup>24–27</sup>

Experimental studies on poly(vinyl alcohol) (PVA) have shown that PVA in aqueous solutions can also inhibit ice growth at temperatures just below 0 °C,<sup>28–31</sup> similar to AFPs, and PVA also shows other properties similar to those of AFP, which is why it is often considered a biomimetic antifreeze molecule.<sup>27,32–34</sup> Moreover, experimental studies have shown that the addition of small amounts of PVA to water droplets leads to an increase in the ice nucleation temperature when compared to the homogeneous ice nucleation temperature of pure water droplets.<sup>33,35,36</sup> While some of these and other authors suggested that PVA acts as a heterogeneous ice nucleator (i.e., a soluble INM),<sup>13,33,35</sup> a recent theoretical study suggested that PVA does not act as a heterogeneous ice nucleator, but instead promotes homogeneous ice nucleation by destabilizing water in the solution due to an accompanying increase in water activity.<sup>37</sup> The aim of our study was to add experimental data that may help to distinguish between these alternative interpretations. Whatever may be the cause, the complementary behavior of ice growth inhibition by PVA around 0 °C on the one hand, and promotion of ice nucleation at temperatures near the homogeneous freezing temperature on the other hand, has already been shown to occur also for IBPs.<sup>10,38</sup> Because of their small size, these IBPs are able to inhibit ice growth by binding to the surface of existing ice crystals and can promote ice nucleation at lower temperatures by acting as rather weak low-temperature ice nucleators. Since these ice nucleating effects only shift the ice nucleation temperature by a few degrees, sensitive experimental methods and very clean samples devoid of ice nucleating impurities are necessary to detect these effects experimentally.<sup>10</sup>

Because of the small size of the investigated aqueous droplet samples and the immersion of the sample droplets in an organic phase, droplet microfluidics experiments are well-suited for this kind of application. Thus, during the last years, several experimental setups were developed to investigate ice nucleation by use of droplet microfluidics.<sup>39–47</sup> In addition to the ability to detect small shifts in the ice nucleation temperature, there are some more advantages of using microfluidics, for example, small sample volumes on the nanoliter scale, decreased impact of contaminations compared to experiments employing larger droplets,<sup>48</sup> and the optical detection of individual droplets' freezing during the experiment for better analysis and statistics.

Microfluidics, in general, is a relatively young field of research, which in recent years has become more and more relevant in biological, ecological, chemical, and engineering sciences.<sup>49–51</sup> In

this article, we describe the development of a modified droplet microfluidics setup that is a follow-up of an existing design termed WISDOM (Weizmann Supercooled Droplets Observation on a Microarray) described previously,<sup>41</sup> which was also a part of larger inter-comparison campaigns employing many different small and large volume experimental setups for ice nucleation studies.<sup>52,53</sup>

In Sec. II, we describe the microfluidic chip fabrication, the temperature calibration of the device, and the experimental procedures of the ice nucleation experiments. In addition, we also describe the chemical synthesis of the surfactant used in the microfluidic device and of the PVA oligomers that were one of the foci of the current investigation.

In Sec. III, we provide a comparison of the ice nucleation results obtained with the device to those obtained with the WISDOM nanoliter droplet microfluidics device on which it is based and to the results of the microliter droplet device Bielefeld Ice Nucleation ARraY (BINARY), which was developed in our laboratory previously.<sup>41,54</sup> We then use this modified device to study the effects of dissolved short- and long-chain PVA samples on the ice nucleation temperature of aqueous nanoliter droplets. With this investigation, we want to answer the question of whether PVA is an INM in the classical sense, that is, whether PVA molecules do indeed act as heterogeneous ice nucleators by stabilizing the critical ice embryo required for ice nucleation, an interpretation suggested by some of the previous experimental studies.<sup>33,35</sup> In contrast, a recent theoretical study suggested that PVA does not act as a heterogeneous ice nucleator but instead promotes homogeneous ice nucleation by destabilizing water in the solution due to an accompanying increase in water activity.<sup>37</sup> This modeling study also suggested that smaller oligomers and even a monomer representative of PVA, propan-2-ol, affect homogeneous ice nucleation very similarly leading to an increase in the ice nucleation temperature of aqueous solutions of monomers and oligomers by about 3 °C, similar to the experimental results of PVA polymers.<sup>33,35</sup>

Therefore, we performed ice nucleation measurements on aqueous solutions of PVA polymers and oligomers of different molar masses and of smaller alcohols, namely, ethanol, propan-2-ol, and 1,3-butanediol, that represent monomers and dimers of PVA. If all of these solutes showed a similar increase in the ice nucleation temperature, this observation would lend support for the homogeneous ice nucleation promotion proposed in the modeling study. On the other hand, a strong decline in ice nucleation enhancement with a decrease in molar mass would rather support the interpretation that PVA acts as a heterogeneous ice nucleator.

## II. MATERIAL AND METHODS

In our droplet microfluidics device, we have made several changes and modifications to the original WISDOM microfluidic setup, on which it is based.<sup>41</sup> Some of the earlier, minor modifications such as employing a different commercial cooling stage and different syringe pumps during the droplet production process were already described in previous studies.<sup>10,17</sup> For the ice nucleation experiments described further below, we have emulsified small aqueous droplets with a volume of about 0.4 nl and a diameter of  $96 \pm 4 \mu\text{m}$  in a continuous oil phase. For the continuous phase, we used the fluorinated oil HFE-7500 (3M, Novec® Engineered Fluid)

to which we added 2 wt. % of the fluorinated surfactant PFPE-Tris, the synthesis of which is described in Sec. II A.<sup>55</sup> The main advantages of this oil-emulsifier system are the larger heat conductivity and the higher stability of the emulsified droplets when compared to mineral oils as well as the simultaneous hydrophobic and lipophobic properties of the continuous oil phase, which decreases the probability of aqueous and in particular organic samples to diffuse into the continuous phase.<sup>42,43,55,56</sup> For comparison, a combination of a mineral oil (M3516; Sigma-Aldrich) and 2 wt. % of the emulsifier Span<sup>®</sup> 80 (Merck) had been used in the WISDOM setup. The droplets were produced in a polydimethylsiloxane-based microfluidic device, with its channels and other structures based on the WISDOM experiment and previous devices.<sup>39,41,57</sup> In Secs. II A–II C, we briefly describe the synthesis of the surfactant, the lithographic processes for chip production, and the temperature calibration of the microfluidic device.

### A. Synthesis of the surfactant PFPE-Tris

According to a procedure described in the literature,<sup>55</sup> PFPE-Tris was synthesized by the conversion of PFPE-COOH with  $\text{SOCl}_2$  into PFPE-COCl and the subsequent reaction of PFPE-COCl with tris(hydroxymethyl)aminomethane (Tris). The molar mass of PFPE-COOH was determined by the addition of a defined amount HFE-7500 (3M, Novec Engineered Fluid) as a reference and integration of the respective signals in the  $^{19}\text{F}$ -NMR spectrum (see the [supplementary material](#), Fig. S1). The workup procedure was modified from the original procedure described in the literature.<sup>55</sup> In contrast to PFPE-Tris, tris(hydroxymethyl)aminomethane is practically insoluble in fluorocarbon oil. Thus, the product was separated from unreacted Tris by extraction with Novec 7100. Undissolved Tris was filtered off, the solvent was removed *in vacuo*, and the extraction process was repeated with HFE-7500. PFPE-Tris was isolated in nearly quantitative yield (99%); see the [supplementary material](#) for more details.

### B. Chip fabrication

The principal structure of the microfluidic channels are based on the WISDOM microfluidic experiment, described in detail previously.<sup>41</sup> In distinction to this previously published setup, we have made some changes to the microfluidic device itself, which are described in Secs. II B and II C, as well as a change in the continuous phase, for which a new surfactant was required, see Sec. II A. We will term this modified WISDOM setup [see Fig. 1(a)] and procedure as the nanoliter Bielefeld Ice Nucleation ARraY (nanoBINARY).

A 3 in. silicon wafer (Siegert Wafer) was immersed in Caro's acid (also known as piranha solution), consisting of one fraction of  $\text{H}_2\text{O}_2$  (30%, VWR Chemicals, AnalaR NORMAPUR) and two fractions of  $\text{H}_2\text{SO}_4$  (95%, Fisher Scientific, Analytic reagent grade), for 5 min and rinsed with water. After repeating the cleaning process, the wafer was dried by spinning at 3000 rpm for 30 s and consecutive heating to 200 °C for 30 min on a hot plate (HT-303 D).

One day before spin-coating, the negative photoresist (Micro Chem, SU-8 3050; a resin that becomes insoluble to the developer solution upon UV radiation, see below) was drawn into a syringe to allow any air bubbles present to settle. A volume of 3 ml of the photoresist was spin-coated (Convac 1001, 1600 rpm, 30 s) onto the wafer. After prebaking on a hotplate (HT-303 D)

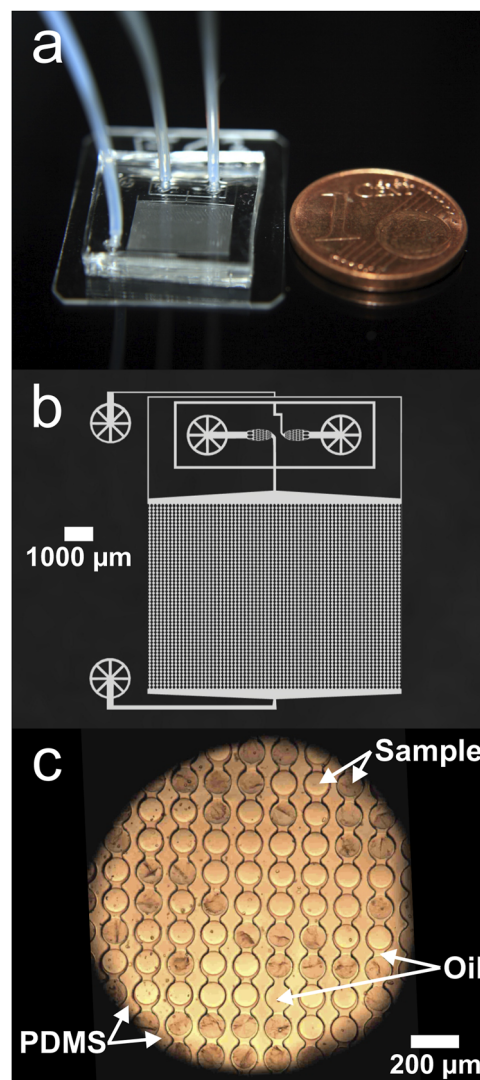


**FIG. 1.** Different images of the nanoBINARY device used for the ice nucleation experiments. (a) Photograph of the microfluidic device with connected tubes and a 1 Euro cent coin for size comparison (coin diameter 16.25 mm). (b) Two-dimensional structures of the channels and the array plotted on the photomask, which are based on the structures of the WISDOM microfluidic device.<sup>41</sup> A more detailed and annotated enlarged view of the central part of the channel structure is given in Fig. S9. (c) Optical microscopy picture of emulsified water droplets (35 frozen, 42 liquid, and one empty spot not containing a droplet, see lower arrow annotated with oil) within the array of the microfluidic device at a temperature of  $-36.2$  °C.

at 95 °C for 45 min, the layer was exposed to UV light for 30 s through a photomask (Selba S. A., Genf) using a mask aligner (Karl Suss, MJB 3). The structures on the photomask [see Fig. 1(b)] had been designed using computer aided design (CAD) Software (Autodesk<sup>®</sup>, AutoCAD 2020) and are very similar to those of the WISDOM microfluidic device and to earlier droplet microfluidics experiments.<sup>39,41,57</sup> The postbake was performed for 1 min at 65 °C and then for 4 min at 95 °C. The wafer with the photoresist

was developed (micro-resist technology, mr-Dev 600) for 25 min. Every 5 min, the wafer was rinsed with small amounts of acetone. After cleaning with acetone and propan-2-ol and drying the wafer, the structures were baked at 65 °C for 5 min and then at 200 °C for 15 min. The height of the structures was measured as  $(108 \pm 2)$   $\mu\text{m}$  using a profilometer (Sloan, Dektak 3030ST). The subsequent silanization of the wafer and the structures was performed by vaporizing 1,1H,1H,2H,2H-perfluorooctyltrichlorosilane (Alfa Aesar, 97%) in a desiccator ( $\sim 100$  mbar) overnight.

For the preparation of the nanoBINARY microfluidic device, the wafer was molded with polydimethylsiloxane (PDMS, DOW Corning, Sylgard® 184, 1:10 w/w). After peeling off the cured PDMS (height of  $\sim 2.5$  mm) from the wafer, the structures of the mold were cut out and the holes for the inlets and the outlet of the channels were produced using a 1.2 mm biopsy punch (WellTech, Rapid-Core). Glass slides (Thermo Scientific, Menzel-Gläser) with a thickness of 0.4 mm and a size of  $20 \times 26$  mm<sup>2</sup> were used as the bottom support for the PDMS pieces containing the microfluidic channels [see Fig. 1(a)]. The molds and the glass slides were cleaned first in double-distilled water and subsequently in propan-2-ol (VWR Chemicals, HiPerSolv CHROMANORM). Both cleaning steps were performed in an ultrasonic device (Elma, Transsonic Digital, 35 kHz). For the assembly, the surface of the glass slide and that of the mold were oxidized in oxygen plasma (Diener electronic Plasma-Surface-Technology GmbH, Zepto) for 25 s at an O<sub>2</sub>-pressure of 2 mbar and a power of 20 W. Thereafter, the two were attached by gently pressing them together.

Before the first use of the freshly prepared microfluidic devices, the channels were hydrophobized by flowing about 100  $\mu\text{l}$  of a liquid hydrophobization agent (Ombrello, Ombrello-Scheibensiegelung) through the channels.

The aqueous droplet production occurs within the structure of the microfluidic device [Fig. 1(b)], when the continuous oil phase and the aqueous phase are merged at specific flow rates at the cross junction of three  $\sim 100$ - $\mu\text{m}$ -wide channels; see the [supplementary material](#), Fig. S9 and Movie M1. The formed droplets are then carried along by the flow into an array consisting of round chambers that are connected by constricting channels, as shown in Fig. 1(c). Once the chambers are filled, the flow is stopped, and the microfluidic chip is disconnected from the tubing and then positioned on the cold stage of an optical microscope for the ice nucleation experiments.

### C. Temperature calibration

For the nanoBINARY freezing experiments, we used an experimental setup consisting of a microscope (Olympus, BX51) and a cold stage (Linkam, BCS 196). The sample droplets were contained in the nanoBINARY device, which was placed on top of the silver block of the cold stage. For better heat conductivity, we applied a thin film of mineral oil (Sigma-Aldrich, Mineral Oil M3516) between the block and the glass slide of the microfluidic device. Since the experimental temperature was measured within the silver block of the cold stage, the actual temperature of the droplets inside the nanoBINARY device was calibrated in a two-step calibration procedure recommended for cooling calibration of calorimeters and already employed previously in our other devices.<sup>40,58</sup> First, we calibrated the cooling and heating rate ( $\beta$ ) dependence at rates of 1, 5,

and 10 °C min<sup>-1</sup> for both cooling and heating. In the second step, we calibrated the equilibrium temperature difference between the droplets and the temperature sensor by extrapolation to a rate of  $\beta = 0$  °C min<sup>-1</sup>. These zero rate thermal equilibrium temperatures were plotted against the equilibrium literature values of several melting, eutectic melting, or freezing points of the different calibration substances and subsequently fitted using a linear function. As a result, we obtained the calibration formula (1) with the experimental temperature  $T_{\text{exp}}$  measured by the sensor, the calibrated temperature  $T$  of the droplets, and the experimental cooling or heating rate  $\beta$ . While the parameters  $a$  and  $b$  have different values for heating and cooling, the parameters  $c$  and  $d$  are fixed and describe the equilibrium temperature deviation,

$$T = \frac{T_{\text{exp}} - \beta \times a - c}{\beta \times b + d}. \quad (1)$$

The values of the parameters  $a$ ,  $b$ ,  $c$ , and  $d$  determined in this way are listed in the [supplementary material](#), Table SI. In the [supplementary material](#), Fig. S3, the deviation of the actual temperatures from the experimental temperatures measured by the sensor is plotted for different cooling and heating rates, and also for the theoretical rate of 0 °C min<sup>-1</sup> representing the equilibrium deviation. All temperatures given below were corrected using Eq. (1) established in the calibration procedure. Moreover, with the resulting temperature uncertainties, also given in Table SI, we calculated a temperature accuracy of  $\pm 0.3$  °C over the entire relevant temperature range from 5 to  $-40$  °C. This uncertainty applies to both, cooling and heating experiments. Further information on the calibration, including the detailed calibration data, is given in the [supplementary material](#).

### D. PVA samples

For the ice nucleation experiments, we used PVA samples of different molar masses and high degrees of hydrolysis. In the figures and text below, the number given after the PVA sample name represents the molar mass  $M$  of the particular sample, that is,  $M = 370$  g mol<sup>-1</sup> for PVA 370. We investigated commercially available samples of PVA polymers with a higher molar mass as well as oligomers with a lower molar mass. It should be noted that the values of  $M$  given for the PVA polymers represent the weight average molar mass, while those for the oligomers represent the number average molar mass, as shown in Table I. The oligomers were synthesized during this study, see below. Moreover, we also investigated low-molecular weight alcohols such as ethanol and propan-2-ol to represent the behavior of a “PVA monomer,” in accordance with a previous molecular dynamics simulation study,<sup>37</sup> and 1,3-butanediol to represent a “PVA dimer;” see the [supplementary material](#), Fig. S13, for a comparison of the structures of these alcohols with that of PVA. All substances used in the ice nucleation experiments described below are listed in Table I together with their molar mass, degree of polymerization, degree of hydrolysis, and their source. For the preparation of all aqueous solutions, we used double-distilled water as the solvent. For the homogeneous ice nucleation reference, we used a sample consisting of pure double-distilled water. All samples were filtered with a syringe filter [SIMPLEPURE, polyethersulfone (PES), 0.22  $\mu\text{m}$ ] before the ice nucleation experiments.

**TABLE I.** Overview of PVA samples and other substances investigated in this study. If available, the molar mass  $M$ , the degree of polymerization  $N_{\text{PVA}}$ ,<sup>a</sup> the value for the degree of hydrolysis, and information about the manufacturer are listed.

Chemical	$M$ (g mol <sup>-1</sup> )	$N_{\text{PVA}}$ <sup>a</sup>	Degree of hydrolysis (mol. %)	Trade name	Manufacturer
Ethanol	46.07	N/A <sup>b</sup>	N/A <sup>b</sup>	AnalaR NORMAPUR, ethanol absolute	VWR Chemicals
Propan-2-ol	60.10	N/A <sup>b</sup>	N/A <sup>b</sup>	HiPerSolv CHROMANORM, 2-propanol	VWR Chemicals
1,3-butanediol	90.12	N/A <sup>b</sup>	N/A <sup>b</sup>	(±)-1,3-butanediol, 99%	Alfa Aesar
PVA 370	370 <sup>c</sup>	~8	100 <sup>d</sup>	N/A <sup>b</sup>	Synthesized in this study as described in Refs. 32 and 59
PVA 420	420 <sup>c</sup>	~10	100 <sup>d</sup>	N/A <sup>b</sup>	
PVA 520	520 <sup>c</sup>	~12	100 <sup>d</sup>	N/A <sup>b</sup>	
PVA 1200	1200 <sup>c</sup>	~27	100 <sup>d</sup>	N/A <sup>b</sup>	
PVA 3900	3900 <sup>c</sup>	~89	100 <sup>d</sup>	N/A <sup>b</sup>	
PVA 27000	27 000 <sup>e</sup>	~613	98.0–98.8	Mowiol® 4-98	Sigma-Aldrich Chemie GmbH
PVA 72000	72 000 <sup>e</sup>	~1635	>98	N/A <sup>b</sup>	N/A <sup>b</sup>
PVA 145000	145 000 <sup>e</sup>	~3292	99.0–99.8	Polyvinyl alcohol 28-99	Fluka Chemie GmbH

<sup>a</sup>The number of monomeric units in a macromolecule or oligomer molecule.<sup>b</sup>N/A: not available or not applicable.<sup>c</sup>For these samples,  $M$  represents the number average molar mass.<sup>d</sup>Acetate groups removed using hydrazine hydrate.<sup>e</sup>For these samples,  $M$  represents the weight average molar mass.

Because PVA is known to form hydrogels upon freezing and thawing, each sample was freshly prepared just before the freezing experiments and used without freeze storing to avoid any effects on the experimental results from a potential formation of such cryogels.<sup>35,60–63</sup> Moreover, experimental observations have shown that gel formation in most of the studied solutions is very unlikely to occur. For example, no precipitate or gel formation was observed in PVA 115000 solutions with a concentration of 1–10 mg ml<sup>-1</sup> after 24 h at temperatures of 20–25 °C or 2–4 °C.<sup>64</sup> Finally, all aqueous PVA solutions employed in this work were filtered through a 0.22 μm syringe filter before the ice nucleation experiments. Thus, the samples are not expected to contain any micro- or macrogels.<sup>65</sup>

The oligomeric samples with a lower molar mass that were used in this work have been synthesized from vinyl acetate by RAFT (reversible addition–fragmentation chain-transfer) polymerization, providing control over the molecular weight and dispersity (ratio of the weight average molar mass to that of the number average molar mass). The molecular weight was tuned by controlling the ratio of the RAFT agent to the monomer. To obtain PVA, the PVAc's were hydrolyzed with hydrazine hydrate (which quantitatively removes the acetate groups), purified by dialysis against MilliQ water and isolated by lyophilization. Detailed descriptions of the synthesis are given in previous publications<sup>32,59</sup> and also in the [supplementary material](#).

## E. Experimental methods for ice nucleation experiments

For the ice nucleation experiments, we used the nanoBI-NARY microfluidic device fabricated in this study (Fig. 1). First, the microfluidic device was filled using two syringe pumps (neMESYS NEM-B101-02 E) with a 100 μl syringe (Hamilton, Gastight® No. 1710) for the aqueous sample, and a 1000 μl syringe (Hamilton, Gastight No. 1001) was used for the continuous fluorinated oil phase. These are connected to the microfluidic device via PTFE tubes (adtech, Bioblock/13) with an inner diameter of 0.56 mm and an outer diameter of 1.07 mm. The continuous phase was filtered (SIMPLEPURE, PES, 0.22 μm) before use. The flow rate for filling the device with the continuous phase was 350 μl min<sup>-1</sup> in all the experiments. The flow rate of the aqueous sample varied between ~150 μl min<sup>-1</sup> for water and aqueous solutions at a small PVA concentration and about ~20 μl min<sup>-1</sup> for the highest concentration of PVA 145000. The aqueous phase and the continuous phase meet at a channel cross junction resulting in the formation of monodisperse droplets in the dripping mode;<sup>66</sup> see the [supplementary material](#), Fig. S9 and Movie M1. With the flow rates outlined previously, the diameter of the resulting droplets is observed to be (96 ± 4) μm [see Fig. 1(c)]. Before each experiment, the microfluidic device was disconnected from the syringes, taking care that the droplets remain in the array and are not influenced by the removal of the tubing.

For the ice nucleation experiments, the filled microfluidic device was placed onto a cold stage (Linkam, BCS 196). The cold stage was mounted on an optical microscope (Olympus, BX51), and an optical magnification factor of 5 was used in all experiments. The corresponding field-of-view allows for the observation of up to 70 individual droplets in a single experimental run [see Fig. 1(c); we note that there are more than a thousand droplets contained in the device]. We performed three individual experimental runs per sample, and before each run, the microfluidic device was refilled with fresh droplets. The droplets were illuminated via the transmission mode of the microscope and observed using a top-mounted digital video camera (QImaging, MicroPublisher 5.0 RTV). During cooling at a rate of  $-1.0\text{ }^{\circ}\text{C min}^{-1}$ , the medium gray value of all pixels related to each particular droplet was determined from the digital images obtained every  $0.1\text{ }^{\circ}\text{C}$ . Based on the changes in gray

values, the freezing events of the droplets can be detected automatically using a LabView software script written for that purpose. The examples of the differences in gray values between liquid and frozen droplets are shown in Fig. 1(c), and additional examples at different temperatures and for other samples are given in Fig. 2(a) and the supplementary material, Fig. S10. The ice melting points of the samples were obtained at a heating rate of  $1.0\text{ }^{\circ}\text{C min}^{-1}$  using the same procedure.

### III. RESULTS AND DISCUSSION

#### A. Exemplary experimental results

Figure 2 shows typical experimental results for ice nucleation data obtained with the nanoBINARY microfluidic device. The optical microscopy images [Fig. 2(a)] show several tens of droplets as they are cooled (from right to left). Liquid droplets (bright) can be easily distinguished from frozen droplets (dark). Three different types of droplet samples are presented: the top row shows the droplets of pure double-distilled water, while the second and third row show aqueous PVA solution samples with concentrations of  $0.1$  and  $5\text{ mg ml}^{-1}$ , respectively, of a PVA sample with a molar mass of  $27\,000\text{ g mol}^{-1}$ . The four images in each row indicate the droplet state at temperatures of  $-30$ ,  $-32.5$ ,  $-35$ , and  $-37.5\text{ }^{\circ}\text{C}$  (from right to left) during cooling at a rate of  $-1\text{ }^{\circ}\text{C min}^{-1}$ . At  $-30\text{ }^{\circ}\text{C}$ , all droplets of each sample are still liquid (i.e., they are bright) and during further cooling, an increasing fraction of droplets become frozen (i.e., dark). At  $-32.5\text{ }^{\circ}\text{C}$ , 11 of the entirely visible droplets of the  $5\text{ mg ml}^{-1}$  PVA sample (bottom row) are already frozen (and 59 remain liquid), while in the other samples, all droplets are still liquid and only freeze at a lower temperature. At  $-37.5\text{ }^{\circ}\text{C}$ , all droplets of each sample are frozen. (It should be noted that a few places in the array are not occupied by a droplet and, thus, they remain bright.) To quantify and compare the fraction of frozen droplets of the different samples, we plot in Fig. 2(b) the resulting frozen fraction curves as  $f_{\text{ice}}(T)$  vs temperature.  $f_{\text{ice}}(T)$  is defined as the cumulative number of frozen droplets  $N_{\text{frozen}}(T)$ , at a specific temperature  $T$ , divided by the total number  $N_{\text{total}}$  of observed droplets in the experiment,

$$f_{\text{ice}}(T) = \frac{N_{\text{frozen}}(T)}{N_{\text{total}}}. \quad (2)$$

As shown in Fig. 2(b), the curves of the PVA solutions are shifted to a higher temperature when compared to that of pure water. At first glance, this is surprising, given that it has been shown that adding solutes to water decreases both the equilibrium ice melting temperature as well as the kinetic homogeneous ice nucleation temperature.<sup>3</sup> However, the observed behavior agrees with previous experimental studies showing that the ice nucleation temperature is increased upon the addition of PVA,<sup>33,35,36</sup> in contrast to other polymers such as poly(ethylene glycol). The  $T_{50}$  values of the samples, defined as the temperature where 50% of the droplets are frozen, i.e.,  $f_{\text{ice}}(T) = 0.5$ , are  $-36.2\text{ }^{\circ}\text{C}$  for water,  $-35.4\text{ }^{\circ}\text{C}$  for the  $0.1\text{ mg ml}^{-1}$  PVA 27000 solution, and  $-33.1\text{ }^{\circ}\text{C}$  for the  $5\text{ mg ml}^{-1}$  PVA solution sample. They are indicated as the small solid circles in each curve with the experimental temperature uncertainty of  $\pm 0.3\text{ }^{\circ}\text{C}$  indicated as error bars. Observing such a small increase in the ice nucleation temperature when compared to pure water is only possible with experimental devices that allow cooling pure water

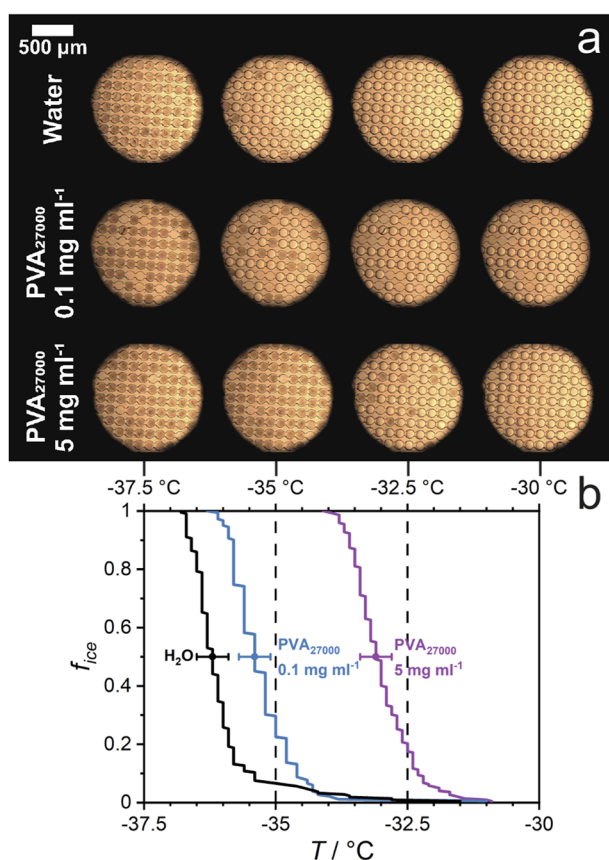


**FIG. 2.** Results of nanoBINARY ice nucleation measurements of double-distilled water and of two aqueous solutions of different concentration of a PVA sample with a molar mass of  $27\,000\text{ g mol}^{-1}$ . (a) These images show the development of the number of unfrozen and frozen droplets upon cooling (from right to left) within the microfluidic device at four different temperatures between  $-30$  and  $-37.5\text{ }^{\circ}\text{C}$ . (b) Frozen fraction  $f_{\text{ice}}(T)$  of droplets shown in panel (a) plotted against the temperature for the two different concentrations of PVA 27000 (colored lines). For comparison, the frozen fraction of double-distilled water (black line) is also shown. The  $T_{50}$  values are indicated as small circles with the temperature uncertainty of the experiment.

samples down to their homogeneous ice nucleation temperature. Microfluidic devices with sub-nanoliter droplet volumes have been shown to be suitable for studying homogeneous ice nucleation in water and aqueous solutions<sup>39–41,45,46,67,68</sup> as well as for determining heterogeneous ice nucleation induced by low-temperature ice nucleators at temperatures just above the homogeneous ice nucleation temperature.<sup>10</sup> For homogeneous ice nucleation in nanoBINARY, a  $T_{50}$  value of  $-36.2^{\circ}\text{C}$  is expected for  $96\ \mu\text{m}$  water droplets at a cooling rate of  $-1^{\circ}\text{C}\ \text{min}^{-1}$ .<sup>69</sup> Freezing devices using larger droplet samples are often subject to heterogeneous freezing processes due to an increased probability of impurities and contact to container walls. For example,  $0.6\ \mu\text{l}$  droplets of pure water studied in the BINARY setup developed in our laboratory<sup>54</sup> show a  $T_{50}$  value of about  $-29.5^{\circ}\text{C}$ , and, therefore, do not allow a clear distinction between the freezing of water and PVA aqueous solution droplets (see the [supplementary material](#), Fig. S7).

## B. Comparison with other devices

In order to evaluate the performance of the nanoBINARY device regarding its ability to quantify homogeneous and heterogeneous ice nucleation processes, we compare it to the WISDOM device on which it is built.<sup>41</sup> Figure 3 shows such a comparison of the frozen fraction curves of droplets containing pure water and aqueous solutions of PVA 27000 from both devices. The agreement between the datasets is very good. Also shown are the frozen fraction curves of birch pollen washing water, which contains highly active ice nucleating molecules,<sup>13,14</sup> again showing the very good agreement between the two devices. The good agreement between the devices that use very different oils and very different surfactants also suggests that the surfactants do not influence the ice nucleation processes in any significant way. Overall, the comparison between nanoBINARY and WISDOM clearly reveals the very

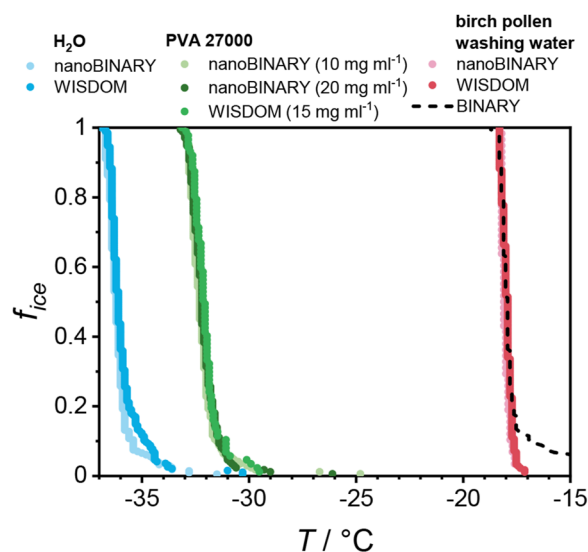


**FIG. 3.** Comparison of  $f_{\text{ice}}(T)$  curves of water (blue points), PVA 27000 (green points), and birch pollen washing water (red points) obtained with the nanoBINARY and WISDOM nanoliter devices. Also shown are the results of birch pollen washing water obtained with the microliter device BINARY. For details, see text.

good agreement and comparability of the two nanoliter freezing devices. This agreement also allows us to at least indirectly compare nanoBINARY to other existing small- and large-volume ice nucleation setups, because WISDOM has shown its ability during participation in several larger ice nucleation intercomparison campaigns.<sup>52,53</sup>

Also shown as the dashed line in Fig. 3 is the frozen fraction curve of larger volume birch pollen washing water droplets ( $0.6\ \mu\text{l}$ ) obtained with the BINARY device. This comparison shows that nanoBINARY and BINARY yield comparable results for highly active, high-temperature ice nucleators, whereas BINARY is not capable of studying less active, low-temperature ice nucleators such as PVA; see the [supplementary material](#), Fig. S7, and the related discussion.

## C. Molar mass dependence of ice nucleation

The observed small shifts in ice nucleation temperatures of a few degrees Celsius upon the addition of PVA shown in Figs. 2 and 3 do not only agree with previous experimental studies for PVAs with a molar mass of  $1700\ \text{g}\ \text{mol}^{-1}$  ( $\sim 39$  mer),<sup>35</sup> but were also predicted by theoretical molecular simulations with the mW water model for smaller oligomers.<sup>37</sup> Interestingly, this modeling study suggests that the observed increase in the ice nucleation temperature in PVA solutions is not due to heterogeneous ice nucleation induced by the PVA macromolecules, but rather due to an enhancement (not reduction!) in the water activity of the solution upon the addition of PVA to water. In fact, water activity values of larger than 1, that is, larger than that of pure water, are predicted at  $2^{\circ}\text{C}$ , both for oligomers (5 mer,  $220\ \text{g}\ \text{mol}^{-1}$ , and 10 mer,  $441\ \text{g}\ \text{mol}^{-1}$ ) and also a monomer representative of PVA, propan-2-ol. Here, we perform the experiments not only with PVA polymers, but also with oligomers as well as molecules representing “PVA monomers” (ethanol and propan-2-ol) and “dimers” (1,3-butanediol), thus providing a more complete dataset that may allow for a better interpretation of the cause for enhanced ice nucleation in aqueous PVA solutions.

As shown in Fig. 4, the frozen fraction curves of four different PVA samples, each at various concentrations, are plotted against temperature, with the molar mass of the studied PVA samples varying from  $370\ \text{g}\ \text{mol}^{-1}$  ( $\sim 8$  mer) to  $145\ 000\ \text{g}\ \text{mol}^{-1}$  ( $\sim 3292$  mer). Figure 4(a) shows the data for the shortest PVA studied, an oligomer with a molar mass of  $370\ \text{g}\ \text{mol}^{-1}$ . The lowest concentration with a measurable effect, that is, a significant increase in  $T_{50}$  when compared to that of pure water considering the experimental temperature uncertainty of  $\pm 0.3^{\circ}\text{C}$ , is  $1\ \text{mg}\ \text{ml}^{-1}$  ( $\Delta T_{50} = 0.4^{\circ}\text{C}$ ), while the effect for the  $5\ \text{mg}\ \text{ml}^{-1}$  solution is significantly stronger ( $\Delta T_{50} = 1.9^{\circ}\text{C}$ ). For the PVA with a molar mass of  $1200\ \text{g}\ \text{mol}^{-1}$  ( $\sim 27$  mer), the smallest concentration with a measurable effect is at  $0.1\ \text{mg}\ \text{ml}^{-1}$  ( $\Delta T_{50} = 0.8^{\circ}\text{C}$ ). While the shift in the ice nucleation temperature increases with the increasing concentration of the PVA, no significant difference in the ice nucleation temperature can be detected for the two highest concentrations of  $10\ \text{mg}\ \text{ml}^{-1}$  ( $\Delta T_{50} = 4.0^{\circ}\text{C}$ ) and  $20\ \text{mg}\ \text{ml}^{-1}$  ( $\Delta T_{50} = 4.2^{\circ}\text{C}$ ). In Figs. 4(c) and 4(d), the data for the commercial PVA samples with molar masses of  $27\ 000\ \text{g}\ \text{mol}^{-1}$  ( $\sim 613$  mer) and  $145\ 000\ \text{g}\ \text{mol}^{-1}$  ( $\sim 3292$  mer) are shown. For both PVAs, there is no ice nucleation effect observed for the lowest concentration of  $0.01\ \text{mg}\ \text{ml}^{-1}$ , and the effect becomes significant for a concentration of  $0.1\ \text{mg}\ \text{ml}^{-1}$ . The ice



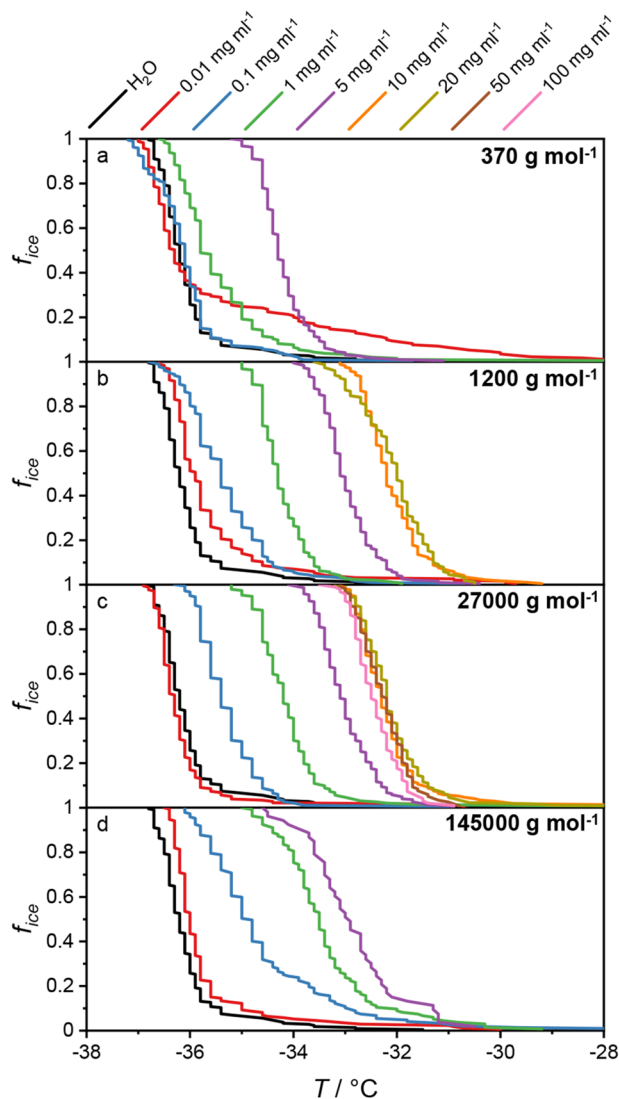


**FIG. 4.** Frozen fraction  $f_{ice}(T)$  of different PVA samples (colored lines) and double-distilled water (black line) as a function of temperature  $T$ . The molar mass of the PVA samples vary from (a)  $370 \text{ g mol}^{-1}$  to (b)  $1200 \text{ g mol}^{-1}$  and (c)  $27\,000 \text{ g mol}^{-1}$  to (d)  $145\,000 \text{ g mol}^{-1}$ . The different PVA concentrations are indicated by color; see the annotation at the top of the figure. We note that in panel (a), the  $f_{ice}(T)$  curve of the  $0.01 \text{ mg ml}^{-1}$  solution (red) increases at higher temperature when compared to more highly concentrated solutions, most likely indicating that some of the droplets contained ice nucleating impurities.

nucleation temperature further shifts to higher temperatures with the increasing concentration for both samples. It should be noted that for PVA 145000, the highest concentration that we were able to investigate was  $5 \text{ mg ml}^{-1}$  ( $\Delta T_{50} = 3.2^\circ\text{C}$ ), because the increasing viscosity with the increasing molar mass and concentration did not allow for a proper droplet preparation in the microfluidic device. For PVA 27000, we were able to measure concentrations of up to  $100 \text{ mg ml}^{-1}$  ( $\Delta T_{50} = 3.7^\circ\text{C}$ ), but an increase in the ice nucleation temperature was only detected until  $10 \text{ mg ml}^{-1}$  ( $\Delta T_{50} = 3.9^\circ\text{C}$ ),

and higher concentrations did not lead to any further increase in the ice nucleation temperature, most likely due to the colligative effect of the high solute concentration, which leads to a reduction in the ice melting temperature and usually also to a concomitant reduction in the homogeneous and heterogeneous ice nucleation temperatures,<sup>3,4</sup> an effect that was also seen in a previous study on PVA.<sup>35</sup>

Figure 5 also shows the frozen fraction curves of the different PVA samples, this time at an equal concentration in each panel. For comparison, double-distilled water and two substances representing a PVA monomer, ethanol and propan-2-ol, as well as one representing a PVA dimer, 1,3-butanediol are also displayed. As shown in Fig. 5(a), no significant change in the ice nucleation activity can be observed in any of the samples at the lowest concentration of  $0.01 \text{ mg ml}^{-1}$ . As shown in Fig. 5(b), a gap can be observed between the freezing curves of two groups of PVA, that is, the PVAs with a molar mass of  $520 \text{ g mol}^{-1}$  ( $\sim 12$  mer) or lower, and those with a molar mass of  $1200 \text{ g mol}^{-1}$  ( $\sim 27$  mer) or higher. While the shorter PVAs with molar masses up to  $520 \text{ g mol}^{-1}$  do not show any significant ice nucleation activity at this concentration, the longer PVAs do show a significant shift of  $T_{50}$ .

For a concentration of  $1 \text{ mg ml}^{-1}$ , all PVAs show a shift in  $T_{50}$  when compared to water, as shown in Fig. 5(c). A clear trend can be observed from the shortest PVA with a molar mass of  $370 \text{ g mol}^{-1}$  ( $\Delta T_{50} = 0.4^\circ\text{C}$ ) to the longest PVA with a mass of  $145\,000 \text{ g mol}^{-1}$  ( $\Delta T_{50} = 2.7^\circ\text{C}$ ). Furthermore, the three monomer and dimer representatives show a shift to lower ice nucleation temperatures when compared to water, suggesting no ice nucleation activity and a reduction in the homogeneous ice nucleation temperature due to colligative effects.<sup>3,4</sup> Finally, as shown in Fig. 5(d), the frozen fractions for the  $5 \text{ mg ml}^{-1}$  sample solutions are plotted. For the shorter PVAs, the shifts in the ice nucleation temperature are much greater than those in the  $1 \text{ mg ml}^{-1}$  solution samples. For the longer PVAs with higher molar masses, the clear trend shown in Fig. 5(c) is not obvious anymore, as it seems that the ice nucleation temperatures are no longer in a consecutive order for higher concentrations and higher molar masses, probably because of the colligative effects of the added solutes on the ice melting temperature and the ice nucleation temperature as suggested previously. Just as observed in Fig. 5(c), only a reduction in the ice nucleation temperature due to the colligative effect has been observed for ethanol, propan-2-ol, and 1,3-butanediol. The weak apparent ice nucleation effect for small values of frozen fractions of 1,3-butanediol appears to be an effect of a contamination because for higher concentration ( $50 \text{ mg ml}^{-1}$ ), this increase was not observed (see the [supplementary material](#), Fig. S11).

For a few samples, we have also measured the frozen fraction curves at a concentration of  $50 \text{ mg ml}^{-1}$ ; see the [supplementary material](#), Fig. S11, which shows that the ice nucleation temperature increase of PVA 27000 is similar to that at  $5 \text{ mg ml}^{-1}$ , while it becomes smaller for some of the smaller oligomers. This is most likely due to the fact that colligative effects on the ice melting temperature and the ice nucleation temperature become stronger at higher concentrations, which has also been observed in a previous study of PVA-induced ice nucleation,<sup>35</sup> decreasing  $\Delta T_{50}$  to smaller values for these samples.

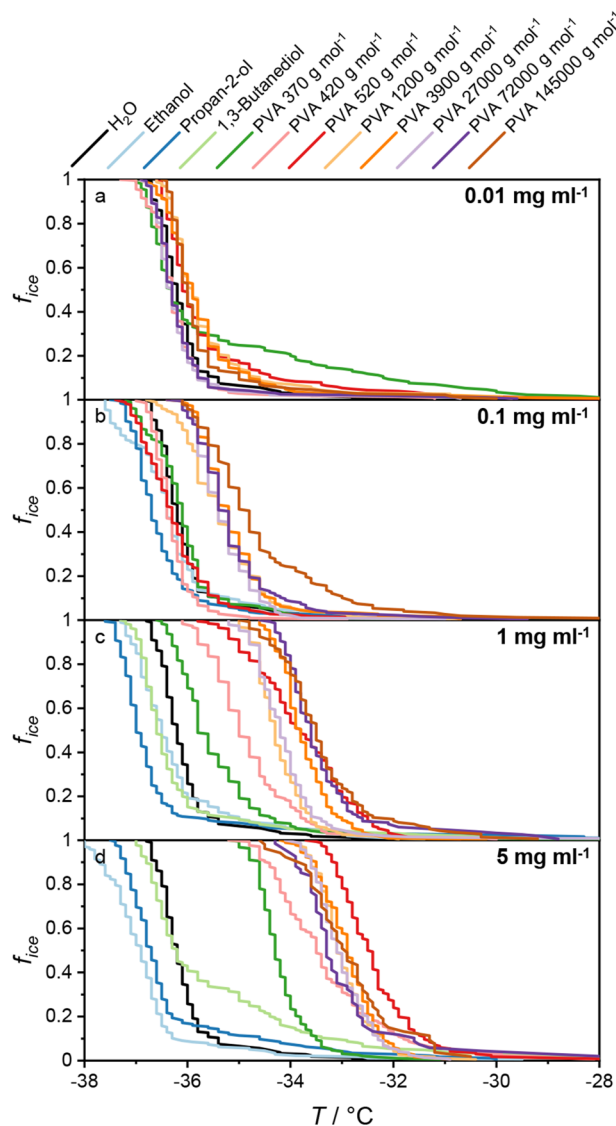


**FIG. 5.** Frozen fraction  $f_{ice}(T)$  of different PVA samples at four particular mass concentrations plotted as a function of temperature  $T$ . For each concentration, PVAs of different lengths are shown (for color coding, see annotation at the top of the figure). In addition, the data of model substances representing the PVA monomer (ethanol and propan-2-ol) and the PVA dimer (1,3-butanediol) as well as those of double-distilled water are also shown for reference. It should be noted that the  $f_{ice}(T)$  curve of the PVA 370 solution (dark green) in panel (a) and that of the 1,3-butanediol solution (light green) in panel (d) increase at higher temperatures when compared to other solutions, most likely indicating that some of the droplets contained ice nucleating impurities.

#### D. Ice nucleation active sites

It is common to compare ice nucleation data or the ice nucleation activity of different substances by plotting the cumulative number of ice nucleating sites per mass  $n_m$ ,<sup>70</sup>

$$n_m = \frac{-\ln(1 - f_{ice})}{c_m \cdot V}. \quad (3)$$

Here,  $V$  is the volume of an individual droplet in the experiment and  $c_m$  is the mass concentration of the ice nucleator (PVA in our case) in the aqueous phase, and so the product  $c_m \cdot V$  represents the total mass of ice nucleators per droplet. We have analyzed the investigated PVA polymers, oligomers, and the dimer and monomers in this manner, and the results are shown in Fig. 6. We have categorized the data into four groups: polymers (dark green in Fig. 6; 3900–145 000 g mol<sup>-1</sup>), oligomers (purple; 370–1200 g mol<sup>-1</sup>), monomers and dimer (orange; ethanol, propan-2-ol, and 1,3-butanediol), and water (black). Figure 6 reveals that the different categories give rise to a different ice nucleation activity as indicated by their different  $n_m$ -versus- $T$  behavior. The polymers show the highest  $n_m$  values and form a rather compact distribution of data points, which suggests that polymers have the same number of ice active sites per mass, independently of their molar mass, see also the supplementary material, Fig. S14. In comparison to the polymers, the oligomers show a slightly reduced ice nucleation activity as their  $n_m$  values are smaller than those of the polymers. Moreover, the distribution of data points is wider and indicates a small molar mass dependence, in which larger oligomers have higher  $n_m$  values and smaller oligomers have lower  $n_m$  values (see the supplementary material, Fig. S15), suggesting that the oligomers become less ice nucleation active on a per mass comparison. Finally, the monomer and dimer representatives ethanol, propan-2-ol, and 1,3-butanediol show a behavior that is very distinct from that of the oligomers and polymers, as their apparent  $n_m$  values are much lower, as shown in Fig. 6. More importantly, however, their behavior does not agree with that of heterogeneous ice nucleators. For example, the  $n_m$  values obtained in solutions of different mass concentrations  $c_m$  of a particular substance do not agree with each other, but the  $n_m$  values in solutions of smaller concentration are larger than those of

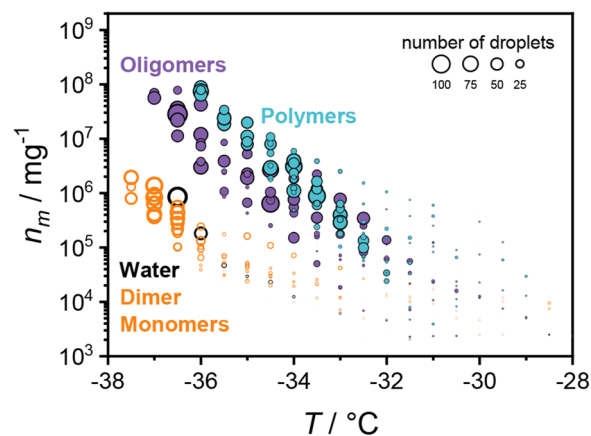


**FIG. 6.** Plot of  $n_m$  vs temperature  $T$ . The individual  $n_m$  values for each substance were combined into four categories: polymers (dark green; 3900–145 000 g mol<sup>-1</sup>), oligomers (purple; 370–1200 g mol<sup>-1</sup>), monomers and dimer (orange; ethanol, propan-2-ol, and 1,3-butanediol), and water (black). The size of the circles indicates the number of droplets that nucleated ice in a particular temperature interval (0.5 °C in width). It should be noted that for all data points labeled open circles, an ice nucleator concentration of 5 mg ml<sup>-1</sup> was assumed independently of the actual concentration of the particular alcohol; see the text and the supplementary material, Fig. S16, for details.

higher concentration by approximately their dilution factor; see the [supplementary material](#), Fig. S16. Such a behavior is indicative of homogeneous ice nucleation occurring in these solutions, and [Fig. 6](#) shows that if we assumed a mass concentration  $c_m$  of  $5 \text{ mg ml}^{-1}$  for all solutions independently of their actual concentration, the data collapse, indicating that the dissolved monomers and dimers are not the ice nucleating agents. In fact, when we assume the same ice nucleator mass concentration  $c_m$  of  $5 \text{ mg ml}^{-1}$  for pure water, the monomer and dimer  $n_m$  values are just below those of pure water, most likely because of colligative effects, i.e., because the addition of the solutes to water leads to a reduced water activity in the solution and, thus, to a reduced ice melting as well as to a reduced ice nucleation temperature.<sup>3,71</sup>

To further support this interpretation, we also performed differential scanning calorimetry (DSC) measurements, in which we compared the behavior of aqueous solutions of the dimer representative, 1,3-butanediol, with that of a polymer, PVA 27000. Even though the two solutions show a similar ice melting point reduction of a few tens of a degree ( $-0.7$  vs  $-0.2$  °C), the ice nucleation temperature of the 1,3-butanediol solution is shifted to a lower temperature by a similar amount ( $-0.5$  °C), in agreement with a homogeneous ice nucleation process, while the ice nucleation in the PVA 27000 solution is elevated by  $4.3$  °C, in agreement with a heterogeneous ice nucleation process; see the [supplementary material](#), Fig. S8, and the related discussion.

Overall, the data and behavior discussed in this section suggest that PVA polymers are heterogeneous ice nucleators, oligomers are also heterogeneous ice nucleators, albeit with a slightly reduced ice nucleation activity on a per mass scale, and the monomer and dimer representatives ethanol, propan-2-ol, and 1,3-butanediol do not show any indication of acting as heterogeneous ice nucleator but rather show the behavior of a typical solute for which the homogeneous ice nucleation temperature is reduced relative to pure water due to the colligative reduction in the water activity of the solution. We observed a size independence of the ice nucleation of polymers and a size dependence of that of the oligomers. This behavior is consistent with the mechanistic view that the ice nucleation activity of a particular molecular ice nucleator should show a size dependence, because a larger INM can support a larger critical ice embryo, thus leading to a higher heterogeneous ice nucleation temperature.<sup>10,13,18</sup> Indeed, such size dependence has been observed also for ice nucleating proteins.<sup>16,17</sup>

### E. Concentration dependence of $\Delta T_{50}$

To better compare the shift in ice nucleation temperatures for the various PVA samples as well as the monomer and dimer samples, we show two different types of plots in [Fig. 7](#), one of the shifts in nucleation temperature  $\Delta T_{50}$  vs PVA mass concentration  $c_m$  [[Fig. 7\(a\)](#)], and the second of  $\Delta T_{50}$  vs PVA molality  $b$  [[Fig. 7\(b\)](#)]. We also included the data of PVA with a molar mass of  $22\,000 \text{ g mol}^{-1}$  from an earlier study.<sup>35</sup> As shown in [Fig. 7\(a\)](#), the data for the PVAs with a molar mass of  $1200 \text{ g mol}^{-1}$  and larger show an overlap for most of the datapoints. On the logarithmic mass concentration scale, the data show a linear increase up to a maximum at a concentration of about  $10 \text{ mg ml}^{-1}$ . Higher concentrations of PVA do not seem to increase the ice nucleation temperature any further, but the values of  $\Delta T_{50}$  begin to decrease again for higher concentrations

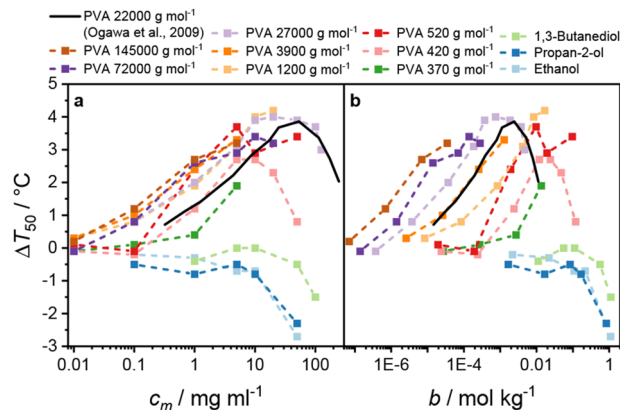


**FIG. 7.** Plots of  $\Delta T_{50}$  against the (a) mass concentration  $c_m$  and (b) molality  $b$  for PVAs with different molar masses from 370 up to  $145\,000 \text{ g mol}^{-1}$  and for ethanol, propan-2-ol, and 1,3-butanediol. For comparison, the solid black line represents data from a previous study.<sup>35</sup> For details, see the text.

due to colligative effects becoming more important as discussed previously. A very similar behavior was observed in the previous study of PVA samples in the range from 1700 to  $93\,000 \text{ g mol}^{-1}$ .<sup>35</sup> In another study, PVA polymers with molar masses from 2000 to  $186\,000 \text{ g mol}^{-1}$  have been investigated.<sup>33</sup> Because the shifts in the ice freezing temperature showed a good overlap, these authors suggested that the ice nucleation efficiency does depend neither on the length nor on the molar concentration of PVA but on the molar concentration of all PVA monomer units contained in the sample. These previous results on PVA polymers are supported by our new experimental observations for PVAs with a molar mass higher than  $1200 \text{ g mol}^{-1}$ . However, here we extended the previous experiments by also studying shorter oligomer samples with smaller molar masses, which show deviating results. As shown in [Fig. 7\(a\)](#), the ice nucleation data of PVA with a molar mass of  $520 \text{ mg ml}^{-1}$  do show an overlap with those of the longer PVAs for concentration of  $1 \text{ mg ml}^{-1}$  and higher. However, PVA 520 does not show any ice nucleation activity at a concentration of  $0.1 \text{ mg ml}^{-1}$ . The same behavior is also observed for the  $\Delta T_{50}$  values of the other oligomers with molar masses of 420 and  $370 \text{ g mol}^{-1}$ . In contrast, the monomer and dimer model substances do not show any significant ice nucleation activity at any of the investigated concentrations in this  $\Delta T_{50}$ -plot, and only a colligative ice nucleation temperature depression is observed at higher concentrations.

In [Fig. 7\(b\)](#), we show the same data as shown in [Fig. 7\(a\)](#) but now plotted against PVA molality  $b$ , which is a unit that is suited to better account for colligative effects. Thus, in this kind of plot, the data depend on the chain length of the PVA molecules. Therefore, a shift of the individual  $\Delta T_{50}$  curves to higher molalities for smaller oligomers is observed, similar to Ref. 35. This is consistent with the observed overlap shown in [Fig. 7\(a\)](#). Furthermore, for the oligomers with a molar mass of  $520 \text{ g mol}^{-1}$  and below, there is no apparent ice nucleation activity at lower molalities, while for higher molalities, the slope is almost the same as that of the longer PVA polymers. The monomer and dimer surrogates again show no ice nucleation activity.

## F. Molar mass dependence of $\Delta T_{50}$

Finally, we created the plots shown in Fig. 8 for a better comparability of the ice nucleation efficiency of the shorter and longer PVA samples. For this purpose, we first fitted the data in the near-linear molality range of Fig. 7(b) (see the supplementary material, Fig. S12), where we consider the ice nucleation data not to be affected by the colligative effects. Using these fit functions, we calculated the molality value  $b$  that would be required for resulting in a particular ice nucleation shift  $\Delta T_{50}$ , for which we chose three representative values of 0.5, 1.0, and 2.0 °C. As shown in Fig. 8(a), the resulting molality values are plotted against the chain length of the respective PVA, expressed as the average number of monomers per chain,  $N_{PVA}$ , i.e., the degree of polymerization. It should be noted that we calculated these chain lengths from  $M$  without considering the molar mass distribution of the samples.

At higher  $N_{PVA}$  values, e.g., longer PVA molecules, the slope of the three curves shown in Fig. 8(a) is nearly identical, just being shifted to higher molality for the higher  $\Delta T_{50}$  values. The four datapoints with the highest  $N_{PVA}$  values, which correspond to the

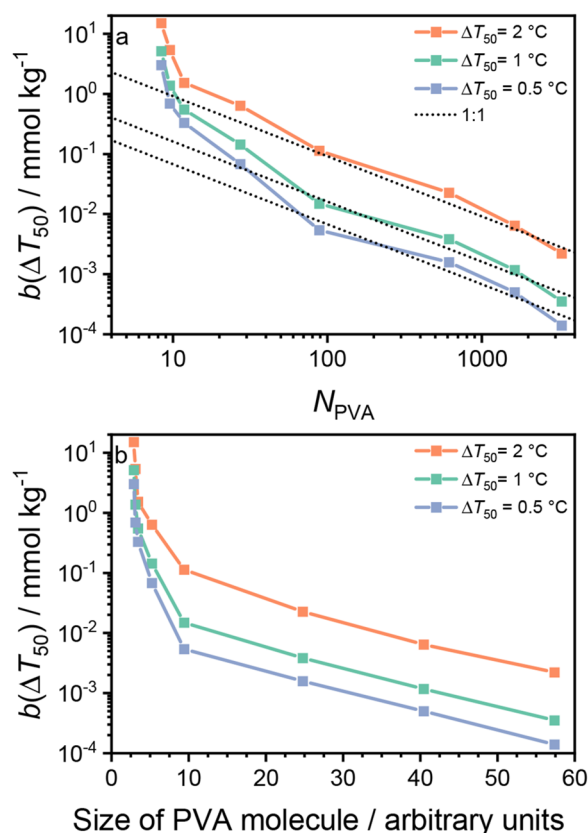


**FIG. 8.** Analysis of the ice nucleation efficiency of different PVAs as a function of their degree of polymerization,  $N_{PVA}$ . (a) Molality  $b$  for different predetermined values of  $\Delta T_{50}$  is plotted against the degree of polymerization,  $N_{PVA}$ , of the PVAs with the different molar masses. The three black-dotted lines indicate a slope of 1:1; for details, see the text. (b) In this panel, the data from (a) are plotted against the size of the PVA molecules in arbitrary units, as estimated from the radius of gyration for an ideal random-coil chain; for details, see the text.

PVA samples with molar masses from  $3900 \text{ g mol}^{-1}$  ( $N_{PVA} = \sim 88.5$  monomers) to  $145\,000 \text{ g mol}^{-1}$  ( $N_{PVA} = \sim 3290$  monomers), reveal a nearly linear behavior in the double-logarithmic plot, as indicated by the three dotted linear lines with a 1:1 slope. This agreement between the data and these dotted lines implies that for the four PVA samples with molar masses from 3900 to  $145\,000 \text{ g mol}^{-1}$ , the ice nucleation activity depends on the total number of monomer units available in a droplet sample. For example, a PVA sample with a molar mass of  $50\,000 \text{ g mol}^{-1}$  ( $N_{PVA} = \sim 1135$  monomers per molecule) at a molar concentration  $c_n$  would lead to the same change in the ice nucleation temperature as a ten times higher concentrated ( $10 \cdot c_n$ ) sample of PVA with a molar mass of  $5000 \text{ g mol}^{-1}$  ( $N_{PVA} = \sim 113.5$  monomers per molecule), as they both result in the same molar concentration of monomers:  $c_n \cdot 1135 = (10 \cdot c_n) \cdot 113.5$ . Hence, this behavior allows the development of a framework for tuning the ice nucleation temperatures of an aqueous droplet as desired by adding a predefined amount of a PVA with an appropriate molar mass.

We note, however, that this relationship is apparently suitable for long-chain PVA samples only but does not apply to the short-chain PVA oligomers, as already seen in the  $n_m$  comparison plot of Fig. 6. The deviation of the data from the dotted 1:1 line increases exponentially with decreasing  $N_{PVA}$  values down to the smallest PVA (molar mass of  $370 \text{ g mol}^{-1}$  corresponding to  $N_{PVA} = \sim 8.4$ ). This behavior agrees with the observations that the monomer and dimer model substances did not show any ice nucleation activity (thus formally requiring an infinite molality, which is unphysical of course).

In Fig. 8(b), we show the same data as shown in Fig. 8(a) but with a modified x-axis. If ice nucleation is indeed induced heterogeneously by the PVA molecules, then the ice nucleation activity should be dependent upon the size  $S$  of the INMs, as has been discussed in detail in previous studies.<sup>10,13,15–19</sup> In aqueous solutions, we expect a random-coil shape of the PVA molecules, specifically for the longer polymer chains. Thus, we can take this shape into account by calculating the size of the random coil from the root of the chain length, i.e.,  $(N_{PVA})^{1/2}$ , representing the scaling of the radius of gyration  $R_g$  for an ideal random-coil chain in an ideal solvent:  $R_g \sim R_0 \cdot (N_{PVA})^{1/2}$ , where  $R_0$  is a constant, which is not known for our particular case.<sup>72</sup> It should be noted that this derivation is valid for the “infinite” chain length.

Indeed, as shown in Fig. 8(b), the relation between the ice nucleation shift  $\Delta T_{50}$  and the random-coil size for the longer PVA samples appears to be even somewhat better than the plot in Fig. 8(a), suggesting that indeed the PVA size is an important parameter for estimating the effect on ice nucleation. This behavior is indicative of the fact that PVA molecules may indeed act as heterogeneous ice nucleators. However, as noted previously, the effect diminishes as the PVA chain length becomes smaller as is the case for the oligomers. The comparisons shown in Fig. 8 suggest a practical limitation for the ice nucleation properties of short-chain PVA oligomers with molar masses of about  $370 \text{ g mol}^{-1}$  and below. These observations seem to be at odds with theoretical simulations that suggested that ice nucleation in aqueous PVA solutions is not heterogeneous, but originates from a destabilization of the supercooled metastable aqueous phase in the presence of PVA, as indicated by an increase in water activity upon the addition of PVA.<sup>37</sup> In contrast, we note that we did not find any evidence for an increase in

water activity, as would be indicated by an increased ice melting temperature. For example, we also performed differential scanning calorimetry measurements of small micrometer-sized emulsified aqueous droplets containing 1,3-butanediol with a concentration of  $10 \text{ mg ml}^{-1}$  and PVA 27000 with a concentration of  $15 \text{ mg ml}^{-1}$ ; see the [supplementary material](#). These measurements did not show any enhanced ice melting point for the two solutions. They also did not show an enhanced ice nucleating activity for 1,3-butanediol, but just a colligative temperature shift of both the ice nucleation temperature as well as the ice melting temperature to lower temperatures relative to double-distilled water; see the [supplementary material](#), Fig. S8. In contrast, PVA 27000 solutions showed a significant increase in ice nucleation temperature despite a reduction in the ice melting temperature. These measurements are consistent with heterogeneous ice nucleation induced by PVA. Furthermore, the PVA ice nucleation simulations suggested also an increase in homogeneous ice nucleation for the monomer propan-2-ol;<sup>37</sup> however, our experiments do not show any evidence for an enhanced ice nucleation for the dimer and monomer representatives 1,3-butanediol, propan-2-ol, and ethanol. Therefore, we argue that our results are more consistent with the suggestion that PVA acts as a heterogeneous ice nucleator.

#### IV. SUMMARY AND CONCLUSIONS

In this work, we introduce the novel experimental microfluidic device nanoBINARY suited for ice nucleation studies, which is based on the previously designed WISDOM device.<sup>41</sup> A comparison of ice nucleation data obtained with the two devices shows very good agreement. Because of the small droplets employed with a diameter of  $(96 \pm 4) \mu\text{m}$  that are emulsified in a fluorinated oil continuous phase, we can study ice nucleation processes down to the homogeneous ice nucleation temperature of water or solutions with this method, as clearly shown when comparing the freezing of various aqueous short- and long-chain PVA solutions with that of either pure water or aqueous solutions of non-active solutes. Thus, it is possible to detect the ice nucleation activity of low-temperature ice nucleators with this method.

We found that the ice nucleating activity of PVA molecules decreases once the chain length becomes smaller than about 88 monomer units and it decreases strongly for oligomers containing less than 12 monomer units. The size dependence of ice nucleation for PVA of different lengths is consistent with previous suggestions for a size dependent activity of INM.<sup>10,13,15–19</sup> However, we cannot exclude that aggregation of PVA molecules may also play a role for their ice nucleation behavior, although such aggregates of flexible linear polymers and oligomers are likely to be different in their local density from the covalently bonded bottle brush PVA polymers, which have a semi-rigid nature.<sup>23</sup> The lowest concentration at which any effect on the ice nucleation temperature could be observed was  $0.1 \text{ mg ml}^{-1}$ . The activity of PVA as an ice nucleating molecule becomes more pronounced with the increasing concentration until concentrations of about  $10 \text{ mg ml}^{-1}$  or higher are reached. We did not observe any enhanced ice nucleation of smaller alcohols representing PVA monomer or dimer units. Overall, our results are consistent with the suggestion that ice nucleation induced in aqueous PVA samples are due to heterogeneous ice nucleation triggered by the PVA polymer and oligomer molecules. In contrast, our

data do not support the suggestion that PVA polymers, oligomers, and even monomers enhance the water activity of the aqueous solutions when compared to water, thereby increasing the homogeneous ice nucleation rate and, thus, shifting the experimentally observed freezing to higher temperature.

#### SUPPLEMENTARY MATERIAL

Details of the chemical synthesis of the PFPE–Tris surfactant and of the PVA samples; details of the temperature calibration, ice nucleation experiments with BINARY and DSC, additional figures; and details as well as a movie of the microfluidic droplet production process are given in the [supplementary material](#).

#### ACKNOWLEDGMENTS

We thank Naama Reicher and Yinon Rudich for their continuous support and helpful contributions during establishing in our laboratory the microfluidic setup described in this article, which is based on their WISDOM experiment. We also thank Anja Diekmann and Marco Annegarn for experimental support and Christian Aleff for the video of the microfluidic droplet production. This project (M.I.G.) received funding from the European Research Council (ERC) under the European Union's Horizon 2020 research and innovation program (Grant Agreement No. 866056) and the Royal Society for an Industry Fellowship (Grant No. 191037) joint with Cytiva.

#### AUTHOR DECLARATIONS

##### Conflict of Interest

The authors have no conflicts to disclose.

##### Author Contributions

T.K. and L.E. performed the conceptualization and the project-administration. C.S. synthesized the PVA oligomer samples with input from M.I.G., and M.K. synthesized the surfactant for the continuous phase in the nanoBINARY experiments with input from B.H. The mold for the PDMS chips were prepared by L.E. and J.D. with input from M.V. L.E. prepared the figures, the writing of the original draft was performed by L.E. and T.K., and M.K., J.D., M.V., D.A., and M.I.G. contributed to the writing by reviewing and editing the original draft.

**Lukas Eickhoff:** Conceptualization (equal); Formal analysis (lead); Investigation (lead); Methodology (equal); Project administration (lead); Validation (lead); Visualization (lead); Writing – original draft (lead); Writing – review & editing (lead). **Mira Keßler:** Investigation (supporting); Methodology (equal); Resources (equal); Visualization (supporting); Writing – review & editing (supporting). **Christopher Stubbs:** Investigation (supporting); Resources (equal). **Jakob Derksen:** Investigation (supporting); Resources (equal); Writing – review & editing (supporting). **Martina Viefhues:** Methodology (equal); Resources (equal); Supervision (equal); Writing – review & editing (supporting). **Dario Anselmetti:** Funding acquisition (equal); Methodology (equal); Project administration (supporting); Resources (equal); Supervision (equal); Writing –

review & editing (supporting). **Matthew I. Gibson:** Funding acquisition (equal); Methodology (equal); Project administration (supporting); Resources (equal); Supervision (equal); Writing – review & editing (supporting). **Berthold Hoge:** Funding acquisition (equal); Methodology (equal); Project administration (supporting); Resources (equal); Supervision (equal). **Thomas Koop:** Conceptualization (equal); Funding acquisition (equal); Methodology (equal); Project administration (lead); Supervision (equal); Writing – original draft (lead); Writing – review & editing (lead).

## DATA AVAILABILITY

The data that support the findings of this study are available from the corresponding author upon reasonable request.

## REFERENCES

- C. A. Angell, *Annu. Rev. Phys. Chem.* **34**, 593 (1983).
- H. R. Pruppacher and J. D. Klett, *Microphysics of Clouds and Precipitation*, 2nd rev. and enl. ed. (Kluwer Academic Publishers, Dordrecht, Boston, 1997).
- T. Koop, B. Luo, A. Tsias, and T. Peter, *Nature* **406**, 611 (2000).
- T. Koop, *Z. Phys. Chem.* **218**, 1231 (2004).
- N. Hiranuma, O. Möhler, K. Yamashita, T. Tajiri, A. Saito, A. Kiselev, N. Hoffmann, C. Hoese, E. Jantsch, T. Koop, and M. Murakami, *Nat. Geosci.* **8**, 273 (2015).
- D. O'Sullivan, M. P. Adams, M. D. Tarn, A. D. Harrison, J. Vergara-Temprado, G. C. E. Porter, M. A. Holden, A. Sanchez-Marroquin, F. Carotenuto, T. F. Whale, J. B. McQuaid, R. Walshaw, D. H. P. Hedges, I. T. Burke, Z. Cui, and B. J. Murray, *Sci. Rep.* **8**, 13821 (2018).
- R. Wagner, L. Ickes, A. K. Bertram, N. Els, E. Gorokhova, O. Möhler, B. J. Murray, N. S. Umo, and M. E. Salter, *Atmos. Chem. Phys.* **21**, 13903 (2021).
- H. Wex, S. Augustin-Bauditz, Y. Boose, C. Budke, J. Curtius, K. Diehl, A. Dreyer, F. Frank, S. Hartmann, N. Hiranuma, E. Jantsch, Z. A. Kanji, A. Kiselev, T. Koop, O. Möhler, D. Niedermeier, B. Nillius, M. Rösch, D. Rose, C. Schmidt, I. Steinke, and F. Stratmann, *Atmos. Chem. Phys.* **15**, 1463 (2015).
- Z. A. Kanji, L. A. Ladino, H. Wex, Y. Boose, M. Burkert-Kohn, D. J. Cziczo, and M. Krämer, *Meteorol. Monogr.* **58**, 1.1–1.33 (2017).
- L. Eickhoff, K. Dreischmeier, A. Zipori, V. Sirotnskaya, C. Adar, N. Reicher, I. Braslavsky, Y. Rudich, and T. Koop, *J. Phys. Chem. Lett.* **10**, 966 (2019).
- N. Reicher, C. Budke, L. Eickhoff, S. Raveh-Rubin, I. Kaplan-Ashiri, T. Koop, and Y. Rudich, *Atmos. Chem. Phys.* **19**, 11143 (2019).
- J. M. Creamean, J. E. Ceniceros, L. Newman, A. D. Pace, T. C. J. Hill, P. J. DeMott, and M. E. Rhodes, *Biogeosciences* **18**, 3751 (2021).
- B. G. Pummer, C. Budke, S. Augustin-Bauditz, D. Niedermeier, L. Felgitsch, C. J. Kampf, R. G. Huber, K. R. Liedl, T. Loerting, T. Moschen, M. Schauerl, M. Tollinger, C. E. Morris, H. Wex, H. Grothe, U. Pöschl, T. Koop, and J. Fröhlich-Nowoisky, *Atmos. Chem. Phys.* **15**, 4077 (2015).
- K. Dreischmeier, C. Budke, L. Wiehemeier, T. Kottke, and T. Koop, *Sci. Rep.* **7**, 41890 (2017).
- M. L. Ling, H. Wex, S. Grawe, J. Jakobsson, J. Löndahl, S. Hartmann, K. Finster, T. Boesen, and T. Šantl-Temkiv, *J. Geophys. Res.: Atmos.* **123**, 1802, <https://doi.org/10.1002/2017jd027307> (2018).
- S. Hartmann, M. Ling, L. S. A. Dreyer, A. Zipori, K. Finster, S. Grawe, L. Z. Jensen, S. Borck, N. Reicher, T. Drace, D. Niedermeier, N. C. Jones, S. V. Hoffmann, H. Wex, Y. Rudich, T. Boesen, and T. Šantl-Temkiv, *Front. Microbiol.* **13**, 872306 (2022).
- J. Forbes, A. Bissoyi, L. Eickhoff, N. Reicher, T. Hansen, C. G. Bon, V. K. Walker, T. Koop, Y. Rudich, I. Braslavsky, and P. L. Davies, *Nat. Commun.* **13**, 5019 (2022).
- Y. Qiu, A. Hudait, and V. Molinero, *J. Am. Chem. Soc.* **141**, 7439 (2019).
- M. Cascajo-Castresana, R. O. David, M. A. Iriarte-Alonso, A. M. Bittner, and C. Marcolli, *Atmos. Chem. Phys.* **20**, 3291 (2020).
- M. I. Gibson, P. G. Georgiou, N. L. H. Kinney, I. Kontopoulou, A. N. Baker, S. A. Hindmarsh, A. Bissoyi, T. R. Congdon, and T. F. Whale, *Biomacromolecules* **23**, 5285 (2022).
- N. H. Fletcher, *J. Chem. Phys.* **29**, 572 (1958).
- B. Zobrist, T. Koop, B. P. Luo, C. Marcolli, and T. Peter, *J. Phys. Chem. C* **111**, 2149 (2007).
- P. G. Georgiou, H. L. Marton, A. N. Baker, T. R. Congdon, T. F. Whale, and M. I. Gibson, *J. Am. Chem. Soc.* **143**, 7449 (2021).
- P. L. Davies, *Trends Biochem. Sci.* **39**, 548 (2014).
- M. Bar Dolev, I. Braslavsky, and P. L. Davies, *Annu. Rev. Biochem.* **85**, 515 (2016).
- A. L. DeVries and D. E. Wohlschlag, *Science* **163**, 1073 (1969).
- I. K. Voets, *Soft Matter* **13**, 4808 (2017).
- C. Budke and T. Koop, *ChemPhysChem* **7**, 2601 (2006).
- P. M. Naullage, L. Lupi, and V. Molinero, *J. Phys. Chem. C* **121**, 26949 (2017).
- F. Bachtiger, T. R. Congdon, C. Stubbs, M. I. Gibson, and G. C. Sosso, *Nat. Commun.* **12**, 1323 (2021).
- C. A. Knight, D. Wen, and R. A. Laursen, *Cryobiology* **32**, 23 (1995).
- T. Congdon, R. Notman, and M. I. Gibson, *Biomacromolecules* **14**, 1578 (2013).
- L. Weng, A. Sweit, and M. Toner, *Cryobiology* **84**, 91 (2018).
- L. Weng, S. L. Stott, and M. Toner, *Langmuir* **34**, 5116 (2018).
- S. Ogawa, M. Koga, and S. Osanai, *Chem. Phys. Lett.* **480**, 86 (2009).
- T. Inada, T. Koyama, F. Goto, and T. Seto, *J. Phys. Chem. B* **115**, 7914 (2011).
- K. Mochizuki, Y. Qiu, and V. Molinero, *J. Am. Chem. Soc.* **139**, 17003 (2017).
- A. Hudait, Y. Qiu, N. Odendahl, and V. Molinero, *J. Am. Chem. Soc.* **141**, 7887 (2019).
- J. F. Edd, K. J. Humphry, D. Irimia, D. A. Weitz, and M. Toner, *Lab Chip* **9**, 1859 (2009).
- B. Riechers, F. Wittbracht, A. Hütten, and T. Koop, *Phys. Chem. Chem. Phys.* **15**, 5873 (2013).
- N. Reicher, L. Segev, and Y. Rudich, *Atmos. Meas. Tech.* **11**, 233 (2018).
- M. D. Tarn, S. N. F. Sikora, G. C. E. Porter, D. O'Sullivan, M. Adams, T. F. Whale, A. D. Harrison, J. Vergara-Temprado, T. W. Wilson, J.-U. Shim, and B. J. Murray, *Microfluid. Nanofluid.* **22**, 52 (2018).
- M. D. Tarn, S. N. F. Sikora, G. C. E. Porter, B. V. Wyld, M. Alayof, N. Reicher, A. D. Harrison, Y. Rudich, J.-U. Shim, and B. J. Murray, *Lab Chip* **20**, 2889 (2020).
- P. Roy, L. E. Mael, T. C. J. Hill, L. Mehndiratta, G. Peiker, M. L. House, P. J. DeMott, V. H. Grassian, and C. S. Dutcher, *ACS Earth Space Chem.* **5**, 1916 (2021).
- C. A. Stan, G. F. Schneider, S. S. Shevkoplyas, M. Hashimoto, M. Ibanescu, B. J. Wiley, and G. M. Whitesides, *Lab Chip* **9**, 2293 (2009).
- T. Brubaker, M. Polen, P. Cheng, V. Ekambaram, J. Somers, S. L. Anna, and R. C. Sullivan, *Aerosol Sci. Technol.* **54**, 79 (2020).
- F. N. Isenrich, N. Shardt, M. Rösch, J. Nette, S. Stavarakis, C. Marcolli, Z. A. Kanji, A. J. deMello, and U. Lohmann, *Atmos. Meas. Tech.* **15**, 5367 (2022).
- M. Polen, T. Brubaker, J. Somers, and R. C. Sullivan, *Atmos. Meas. Tech.* **11**, 5315 (2018).
- G. M. Whitesides, *Nature* **442**, 368 (2006).
- S. Täuber, C. Golze, P. Ho, E. von Lieres, and A. Grünberger, *Lab Chip* **20**, 4442 (2020).
- X. Zhu, K. Wang, H. Yan, C. Liu, X. Zhu, and B. Chen, *Environ. Sci. Technol.* **56**, 711–731 (2022).
- P. J. DeMott, O. Möhler, D. J. Cziczo, N. Hiranuma, M. D. Petters, S. S. Petters, F. Belosi, H. G. Bingemer, S. D. Brooks, C. Budke, M. Burkert-Kohn, K. N. Collier, A. Danielczok, O. Eppers, L. Felgitsch, S. Garimella, H. Grothe, P. Herenz, T. C. J. Hill, K. Höhler, Z. A. Kanji, A. Kiselev, T. Koop, T. B. Kristensen, K. Krüger, G. Kulkarni, E. J. T. Levin, B. J. Murray, A. Nicosia, D. O'Sullivan, A. Peckhaus, M. J. Polen, H. C. Price, N. Reicher, D. A. Rothenberg, Y. Rudich, G. Santachiara, T. Schiebel, J. Schrod, T. M. Seifried, F. Stratmann, R. C. Sullivan, K. J. Suski, M. Szakáll, H. P. Taylor, R. Ullrich, J. Vergara-Temprado, R. Wagner, T. F. Whale, D. Weber, A. Welti, T. W. Wilson, M. J. Wolf, and J. Zenker, *Atmos. Meas. Tech.* **11**, 6231 (2018).
- N. Hiranuma, K. Adachi, D. M. Bell, F. Belosi, H. Beydoun, B. Bhaduri, H. Bingemer, C. Budke, H.-C. Clemen, F. Conen, K. M. Cory, J. Curtius,

- P. J. DeMott, O. Eppers, S. Grawe, S. Hartmann, N. Hoffmann, K. Höhler, E. Jantsch, A. Kiselev, T. Koop, G. Kulkarni, A. Mayer, M. Murakami, B. J. Murray, A. Nicosia, M. D. Petters, M. Piazza, M. Polen, N. Reicher, Y. Rudich, A. Saito, G. Santachiara, T. Schiebel, G. P. Schill, J. Schneider, L. Segev, E. Stopelli, R. C. Sullivan, K. Suski, M. Szakáll, T. Tajiri, H. Taylor, Y. Tobo, R. Ullrich, D. Weber, H. Wex, T. F. Whale, C. L. Whiteside, K. Yamashita, A. Zelenyuk, and O. Möhler, *Atmos. Chem. Phys.* **19**, 4823 (2019).
- <sup>54</sup>C. Budke and T. Koop, *Atmos. Meas. Tech.* **8**, 689 (2015).
- <sup>55</sup>Y.-L. Chiu, H. F. Chan, K. K. L. Phua, Y. Zhang, S. Juul, B. R. Knudsen, Y.-P. Ho, and K. W. Leong, *ACS Nano* **8**, 3913 (2014).
- <sup>56</sup>3M Company, Novec 7500 Engineered Fluid. Product Information, <https://multimedia.3m.com/mws/media/65496O/3m-novec-7500-engineered-fluid.pdf>.
- <sup>57</sup>C. H. J. Schmitz, A. C. Rowat, S. Köster, and D. A. Weitz, *Lab Chip* **9**, 44 (2009).
- <sup>58</sup>S. M. Sarge, G. W. H. Höhne, H. K. Cammenga, W. Eysel, and E. Gmelin, *Thermochim. Acta* **361**, 1 (2000).
- <sup>59</sup>T. Congdon, P. Shaw, and M. I. Gibson, *Polym. Chem.* **6**, 4749 (2015).
- <sup>60</sup>N. A. Peppas, *Makromol. Chem.* **176**, 3433 (1975).
- <sup>61</sup>M. Komatsu, T. Inoue, and K. Miyasaka, *J. Polym. Sci., Part B: Polym. Phys.* **24**, 303 (1986).
- <sup>62</sup>C. M. Hassan and N. A. Peppas, *Macromolecules* **33**, 2472 (2000).
- <sup>63</sup>I. Kontopoulou, T. R. Congdon, S. Bassett, B. Mair, and M. I. Gibson, *Polym. Chem.* **13**, 4692 (2022).
- <sup>64</sup>L. G. Damshkaln, I. A. Simenel, and V. I. Lozinsky, *J. Appl. Polym. Sci.* **74**, 1978 (1999).
- <sup>65</sup>P. Verdugo, *Annu. Rev. Mar. Sci.* **4**, 375 (2012).
- <sup>66</sup>P. Zhu and L. Wang, *Lab Chip* **17**, 34 (2017).
- <sup>67</sup>L. Weng, S. N. Tessier, K. Smith, J. F. Edd, S. L. Stott, and M. Toner, *Langmuir* **32**, 9229 (2016).
- <sup>68</sup>N. Shardt, F. N. Isenrich, B. Waser, C. Marcolli, Z. A. Kanji, A. J. deMello, and U. Lohmann, *Phys. Chem. Chem. Phys.* **24**, 28213 (2022).
- <sup>69</sup>T. Koop and B. J. Murray, *J. Chem. Phys.* **145**, 211915 (2016).
- <sup>70</sup>B. J. Murray, D. O'Sullivan, J. D. Atkinson, and M. E. Webb, *Chem. Soc. Rev.* **41**, 6519 (2012).
- <sup>71</sup>T. Koop and B. Zobrist, *Phys. Chem. Chem. Phys.* **11**, 10839 (2009).
- <sup>72</sup>J. E. Kohn, I. S. Millett, J. Jacob, B. Zagrovic, T. M. Dillon, N. Cingel, R. S. Dothager, S. Seifert, P. Thiyagarajan, T. R. Sosnick, M. Z. Hasan, V. S. Pande, I. Ruczinski, S. Doniach, and K. W. Plaxco, *Proc. Natl. Acad. Sci. U. S. A.* **101**, 12491 (2004).